Clays and Clay Minerals, Vol. 49, No. 3, 204–215, 2001.

FORMATION AND GROWTH OF SMECTITES IN BENTONITES: A CASE STUDY FROM KIMOLOS ISLAND, AEGEAN, GREECE

GEORGE E. CHRISTIDIS

Technical University of Crete, Department of Mineral Resources Engineering, 73100 Chania, Greece

Abstract—The low-temperature alteration of a rhyolitic rock from Kimolos Island, Aegean, Greece, yielded an alteration profile characterized by gradual transition from fresh glass to bentonite containing homogeneous Chambers-type montmorillonite and then to a mordenite-bearing bentonite. Both mordenite and smectite were formed from poorly crystalline precursors, which probably had compositions comparable to that of the crystalline end-product. However, their composition may have been modified to some degree after reaction with the fluid phase. Particle length and width measurements of smectite crystals yielded lognormal profiles, which suggest supply-controlled crystal growth in an open system or random ripening in a closed system. The former mechanism is in accordance with the observed sustained supply of Mg and Fe by the fluid phase throughout the alteration profile and is believed to be the dominant formation mechanism of smectites in bentonites in general. In the mordenite-bearing zone, random ripening is expected in domains with low permeability, in which the system was essentially closed, favoring the formation of mordenite. The level of supersaturation with respect to smectite was probably lower in the mordenite-bearing zone. Smectite probably affected pore-fluid chemistry either through ion exchange or via dissolution of initially formed K-bearing smectite. The latter process raised the $K^+/(Na^+ + Ca^{2+})$ activity ratio of the pore-fluid favoring K-bearing mordenite.

Key Words—Bentonite, Crystal Growth, Montmorillonite, Mordenite, Open System, Particle-Size Distribution, Precursor, Random Ripening.

INTRODUCTION

The alteration of volcanic glass to smectite and zeolites is a common process, which often yields bentonite or zeolite deposits (Iijima, 1980; Senkayi *et al.*, 1984; Hay and Guldman, 1987; Altaner and Grim, 1990; Christidis *et al.*, 1995). This process may take place through vapor-phase crystallization, burial diagenesis, contact metamorphism, hydrothermal activity, percolating groundwater, in alkaline lakes or on the sea floor in marine sediments (Iijima, 1980; Cas and Wright, 1988). Vapor phase crystallization, often associated with welding of ignimbrites, is of theoretical significance and does not produce significant amounts of zeolites (Cas and Wright, 1988).

The factors controlling the alteration of volcanic glass are Si activity, pH, alkalinity, the activity of alkalis and alkaline earth elements, temperature, pressure and the partial pressure of H_2O (Hay, 1977; Iijima, 1980). Leaching of alkalis and a high Mg activity promote the formation of smectite (Hay, 1977; Senkayi *et al.*, 1984). When leaching is not effective, zeolites crystallize, usually from precursor gels (Mariner and Surdam, 1970; Steefel and van Cappellen, 1990). Smectite generally forms in the initial stages of the alteration, where the $(Na^+ + K^+)/H^+$ activity ratio of the fluid phase is low (Sheppard and Gude, 1973; Hay and Guldman, 1987). High ratios of $(Na^+ + K^+)/H^+$ activity favor the formation of zeolites instead of smectite (Hess, 1966). Smectite has been reported to form from poorly crystalline precursors in various environments and in the laboratory (Zhou and Fyfe, 1989; Banfield and Eggleton, 1990; Kawano and Tomita, 1992), although the existence of a precursor phase is not always necessary (Banfield *et al.*, 1991).

The type and composition of the zeolites formed is controlled primarily by the chemical composition of the parent rock (Iijima, 1980). Most alkaline zeolites like clinoptilolite, mordenite and phillipsite are converted to more stable phases like analcime and/or alkaline feldspars at higher temperature, pressure, alkalinity and salinity, both in nature and in the laboratory (Boles, 1977; Hay, 1977; Hawkins, 1981; Bowers and Burns, 1990). In contrast, only limited information about a systematic relationship between the chemical composition of the neoformed phases and the chemistry of the parent rock has been reported for smectites. In general, Mg-Fe smectites like Wyoming type, Chambers type and Fe-rich montmorillonite tend to form from andesitic-dacitic precursors, whereas rhyolitic protoliths yield Al-rich smectites like beidellite and Tatatilla type montmorillonite (Christidis and Dunham, 1993, 1997). Exceptions to this trend have been reported however, *e.g.* formation of Chambers-type montmorillonite was observed during alteration of rhyolitic rocks to bentonite (Christidis, 1998a).

Recent simulation of crystal growth in thermodynamically open and closed systems has shown that it may be possible to deduce geological history from a measured crystal-size distribution for minerals (Eberl *et al.*, 1998). This deduction is based on the particle-thickness distribution of the clay fraction determined by the Bertaut-Warren-Averbach (BWA) technique. To

Copyright © 2001, The Clay Minerals Society

https://doi.org/10.1346/CCMN.2001.0490303 Published online by Cambridge University Press

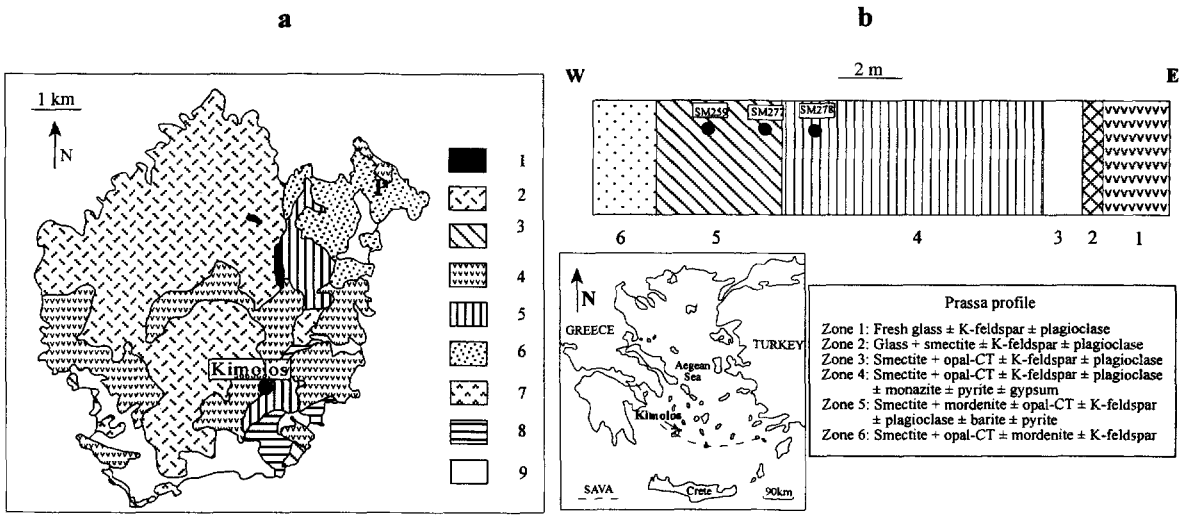

Figure 1. (a) Simplified geological map of the Kimolos Island modified after Fyticas and Vougioukalakis (1993). Key to the numbers: 1—Granite, 2—Kastro ignimbrite, 3—Hydrothermally-altered volcanic rocks, 4—Undifferentiated lavas, 5—Pyroclastic breccia, 6—Ignimbrite of the Prassa area, 7—Pumice flows, 8—Pyroclastics of the Psathi area, 9—Alluvial scree and eluvial deposits, P—Prassa deposit. (b) Schematic cross section of the Prassa deposit, Kimolos (after Christidis, 1998a): The numbers refer to the different alteration zones. Zone 1—glass; zone 2—glass + smectite; zone 3—smectite + opal-CT; zone 4—smectite; zone 5—smectite + mordenite ± opal-CT; zone 6—smectite + opal-CT ± mordenite. Igneous plagioclase and K-feldspar are present in all alteration zones. SM259, SM277 and SM278 are the samples whose particle-size distributions were determined.

date, there have been no studies of growth mechanisms of smectites in bentonites using this technique.

Although smectites and zeolites are usually associated in nature, no attempt has been made to examine interdependence of their chemistry and the chemistry of the associated pore-fluids during formation. Christidis and Scott (1997) and Christidis (1998a) described the progressive alteration of an acidic rock from Kimolos Island, Greece, to smectite ± mordenite by seawater, and they calculated water : rock ratios during alteration based on mass balance calculations. The purpose of the present work was: (1) to study the formation mechanism of smectite and mordenite; (2) to gain a greater understanding of the crystallization mechanism of smectite and the possible influence of zeolites; and (3) to discuss the possible control that smectite and zeolites might exert on the pore-fluid chemistry.

LOCATION AND GEOLOGICAL SETTING

The Island of Kimolos is situated in the southwestern part of the Cyclades Islands in the Aegean Sea, Greece and constitutes part of the South Aegean Volcanic Arc (Figure 1), which was created by the subduction of the African Plate under the deformed margin of the Eurasian Plate (Fyticas *et al.*, 1986). The geological and volcanological characteristics of Kimolos (Figure 1) were described by Fyticas and Vougioukalakis (1993). The study area is the Prassa bentonite deposit, located in the southeastern part of the Island (Figure 1).

MATERIALS AND METHODS

Bentonite samples were collected from an alteration profile described by Christidis and Scott (1997) and Christidis (1998a), of the Prassa Ignimbrite, consisting of six different alteration zones (Figure 1). The mineralogy was determined by X-ray diffraction (XRD) using a Philips diffractometer equipped with a PW1710 control unit, operating at 40 kV and 30 mA, using Ni-filtered CuKα radiation. The scanning speed was 1°2θ/min. After dispersion of the rock in distilled water using Na polyphosphate deflocculant, the <2 μm fraction was separated, and dried at atmospheric conditions onto glass slides. The slides were then saturated with ethylene glycol at 60°C for at least 16 h, to ensure maximum solvation.

The smectite and mordenite chemistry was determined by electron microprobe analysis of epoxy impregnated polished blocks, using a JEOL JXA-8600 Superprobe, and a Link Series I energy dispersive spectrometer (EDS). The conditions used for smectite analysis were described by Christidis and Dunham (1993). The same conditions were used for zeolites except for the use of a defocused beam (20 μm *vs.* 5 μm used for smectites) and a shorter count time (25 s *vs.* 100 s used for smectites). The areas for analysis were selected carefully using back-scattered electron images to avoid contamination by Ti and Fe oxides and sulfides and to distinguish smectite from mordenite. The analyses of zeolite considered the error factor

https://doi.org/10.1346/CCMN.2001.0490303 Published online by Cambridge University Press

Table 1. Microprobe analyses and structural formulae of smectites from the Prassa deposit, Kimolos.

	1 zone 5	2 zone 5	3 zone 5	4 zone 4	5 zone 4	6 zone 4	7 zone 3	8 zone 3
SiO_2	50.98	50.86	53.25	53.79	63.55	60.69	60.38	62.16
Al_2O_3	18.02	18.31	19.18	19.20	21.85	20.82	21.02	22.42
Fe_2O_3	1.66	1.68	2.06	1.71	1.27	1.56	1.66	1.82
MgO	4.06	4.21	3.62	4.13	5.07	4.21	4.78	4.84
CaO	0.71	0.85	1.62	1.43	1.25	1.00	1.27	0.85
Na_2O	0.57	0.53	0.42	0.57	0.47	0.41	0.45	0.73
K_2O	0.75	1.03	0.27	0.00	0.00	0.00	0.00	0.00
Total	76.75	77.47	80.42	80.83	93.46	88.69	89.56	92.82
				Structural formulae based on 11 oxygens				
				Tetrahedral cations				
Si	3.91	3.88	3.89	3.90	3.96	3.98	3.94	3.91
Al^{IV}	0.09	0.12	0.11	0.10	0.04	0.02	0.06	0.09
				Octahedral cations				
Al^{VI}	1.53	1.52	1.55	1.54	1.57	1.59	1.55	1.57
Fe^{3+}	0.10	0.10	0.11	0.09	0.06	0.08	0.08	0.09
Mg	0.42	0.42	0.39	0.42	0.42	0.38	0.42	0.39
				Interlayer cations				
Ca	0.06	0.07	0.13	0.11	0.08	0.07	0.09	0.06
Na	0.08	0.08	0.06	0.08	0.06	0.05	0.06	0.09
K	0.07	0.10	0.03	0.00	0.00	0.00	0.00	0.00
Mg	0.04	0.04	0.00	0.03	0.05	0.03	0.05	0.06
L. charge	0.36	0.40	0.35	0.37	0.31	0.25	0.33	0.33
I. charge	0.35	0.40	0.35	0.36	0.32	0.25	0.34	0.33

Exchangeable Mg was calculated by assuming the total number of octahedral cations to be 2.05 (average value of Grim and Güven, 1978). L. charge = layer charge, I. charge = interlayer charge.

$E = 100[(Al + Fe) - (Na + K) - 2(Ca + Mg)]/[(Na + K) + 2(Ca + Mg)]$ (Gottardi and Galli, 1985). Analyses with $E \geq \pm 10\%$ were discarded. Smectite analyses with totals <70% were discarded following the reasoning of Christidis and Dunham (1993).

Gold-coated broken surfaces of representative samples were examined with a Hitachi S520 scanning electron microscope (SEM), equipped with a Link AN1000 energy dispersive spectrometer (EDS) for qualitative analyses. The <1 μm clay fractions of three samples (SM278, SM277 and SM259) from the smectite and the smectite + mordenite zone (Figure 1) were dispersed in distilled water using Na polyphosphate (1 mg clay/40 mL of water), spread on copper grids, allowed to dry, coated with carbon, and examined with a JEOL 100CX transmision electron microscope (TEM). To avoid disruption of the smectite flakes, ultrasonic vibration was not used for sample disaggregation. This sample treatment does not change the morphology of delicate smectite flakes. For >200 smectite particles from each sample, length and width measurements (larger and smaller dimension, respectively) were made on a digitizing table, using a computer program written by Dr A. Low (Biology Department, University of Leicester).

RESULTS

Mineralogy and mineral chemistry

Smectite. The main mineral phase present in all alteration zones is dioctahedral smectite, which has been characterized as Chambers type and Tatatilla type montmorillonite (*e.g.* Güven, 1988). Mixed-layer illite-smectite was not detected by XRD. Unlike the smectites from Milos (Christidis and Dunham, 1993, 1997), these smectites have limited compositional variation (Table 1, Figure 2), which may be attributed to limitations of the analytical method used (Warren and Ransom, 1992). Accessory authigenic monazite, barite and gypsum crystals dispersed through the mass of the altered rock were detected only by SEM.

The smectites display a general negative trend between Si and total Al, and between ^{VI}Al and Fe^{3+} (Figure 3). A similar trend is observed between ^{VI}Al and Mg when the total number of octahedral cations is taken as 2.05, *i.e.* the average value for octahedral cations in smectite formulae after Grim and Güven (1978). For comparison, the chemistry of smectites derived from similar rocks at Milos Island is dominated mainly by a negative trend between Si and Al and to a lesser degree between ^{VI}Al and Mg (Christidis and Dunham, 1997). These chemical trends are not obvious in the smectites examined in this study, because all of the trends display scattering (Figure 3). In contrast, a negative relationship between Fe and ^{VI}Al is observed, which is characteristic of smectites derived from intermediate rocks (Christidis and Dunham, 1993).

In the mordenite-bearing zone (zone 5), the smectites are low in Si and Mg and richer in Fe^{3+} relative

https://doi.org/10.1346/CCMN.2001.0490303 Published online by Cambridge University Press

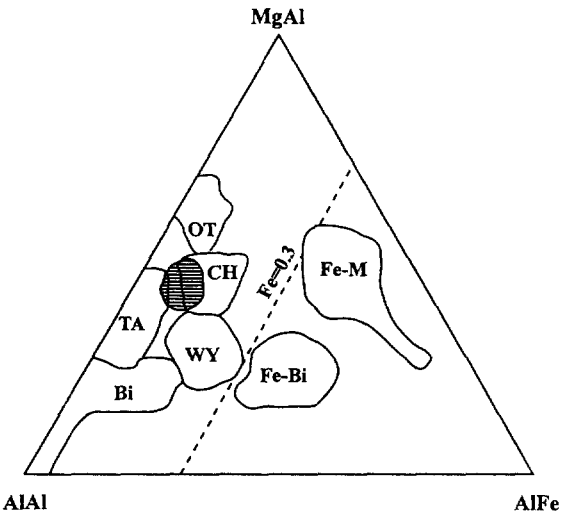

Figure 2. Projection of the smectites from the smectite- and the mordenite-bearing zones (shaded area) following the diagram of Güven (1988). Bi = beidellite, TA = Tatatilla montmorillonite, Ch = Chambers montmorillonite, WY = Wyoming montmorillonite, OT = Otay montmorillonite, Fe-Bi = Fe-rich beidellite, Fe-M = Fe-rich montmorillonite. The line at 0.3 Fe^{3+} atoms separates the Fe-rich from the Fe-poor dioctahedral smectites.

to their counterparts from zones 3 and 4 (Figure 3, Table 1). Moreover, they show a negative trend between K and the remaining interlayer cations (Figure 4a). Due to analytical constraints imposed by microprobe analysis, it is not certain whether K is exchangeable or fixed. However, it has been shown that the materials studied have improved swelling properties and develop high viscosity after Na exchange (Christidis, 1998b). This suggests that K is exchangeable. The lower Si content is related to the presence of abundant Si-rich mordenite. The greater Fe^{3+} content is attributed to the presence of smectite, the major Fe-bearing neoformed phase, which occurs in near equal amounts as the Fe-free mordenite.

Mordenite. Two varieties of mordenite were recognized on the basis of exchangeable cations: a Na,Ca-rich (common) variety and a K-bearing mordenite (Table 2). The Si/Al ratio of each variety varies from 4.86–5.8. As expected, a negative relationship occurs between K and the remaining exchangeable cations (Figure 4b), indicating that, similar to smectites, K is competing with the other exchangeable cations. The chemical variation of the exchangeable sites is determined mainly by the variation between Na and K, whereas the importance of Mg is minimal (Figures 4b, 5).

Mineral textures

Smectite. As determined by SEM, smectite occurs in the form of wavy flakes, often forming characteristic

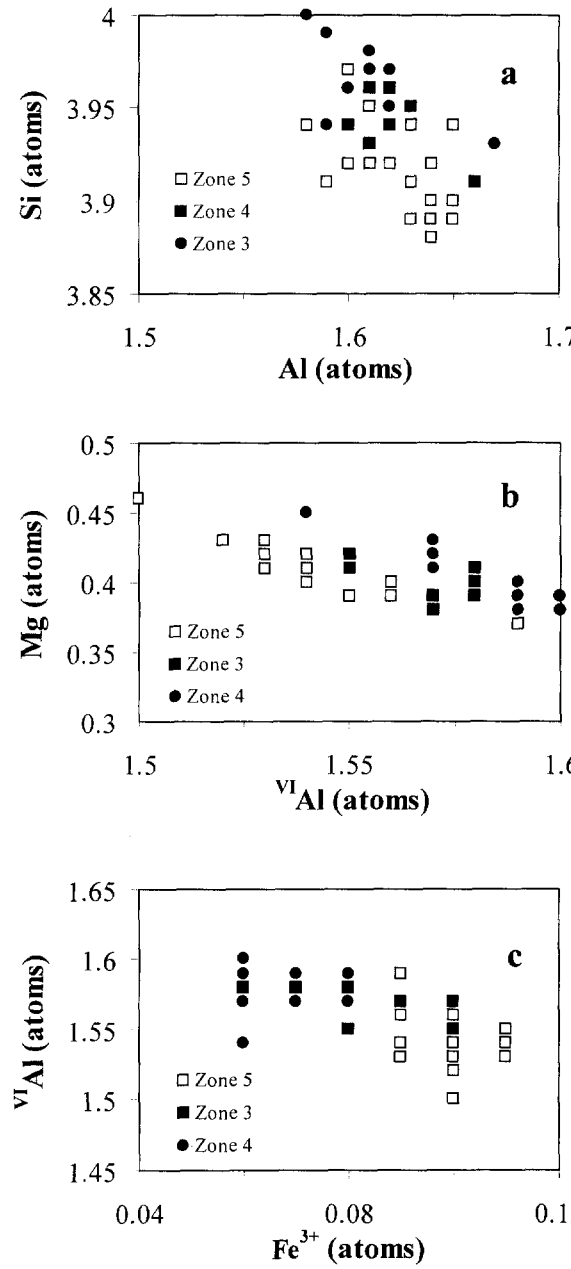

Figure 3. Compositional characteristics of smectites from the Prassa deposit, observed from plots between: (a) Si and total Al; (b) octahedral Al and Mg; and (c) octahedral Al and Fe^{3+}.

honeycomb textures and pseudomorphic textures over the parent glass (Figure 6a, c). No systematic relationship between the smectite morphology and the location of the flakes relative to the glass shards was observed (Figure 6b). Smectite crystals formed at the expense of volcanic glass through a precursor phase (Figure 7). Semi-quantitative EDS analysis showed that this precursor-intermediate phase has a larger Al content and

https://doi.org/10.1346/CCMN.2001.0490303 Published online by Cambridge University Press

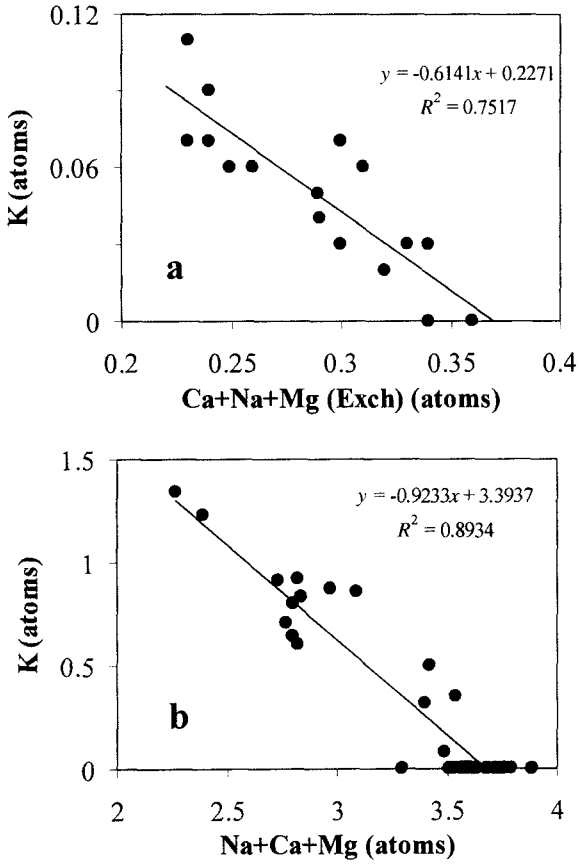

Figure 4. Relationship between K and the remaining exchangeable cations observed (a) in smectites and (b) in mordenites from the mordenite-bearing zone of the Prassa deposit. Mg (exch) = exchangeable Mg calculated by assuming that the total number of octahedral cations is 2.05.

smaller Si, Mg and Fe contents compared to the volcanic glass, *i.e.* its composition could approach the allophane-type phase described by Kawano and Tomita (1992). Due to analytical limitations and the small particle size of the precursor phase, it cannot be determined whether Fe and Mg are present in the precursor phase or in the surrounding glass. Formation of smectite at the expense of igneous feldspars, although common in Milos (Christidis *et al.,* 1995), is not often seen in this alteration profile.

As observed using TEM, smectites occur mainly as subhedral particles, and to a lesser degree as lath-shaped and euhedral particles with polygonal outlines (Güven and Pease, 1975; Grim and Güven, 1978). The euhedral crystals form foliated and compact lamellar aggregates (Grim and Güven, 1978) with face-to-face association. The lath-shaped smectites form mainly by gentle folding of the edges of thin lamellae, although crystals with unfolded edges are also common.

Mordenite. Mordenite, which in general postdates smectite, has a fibrous habit, and a length:width ratio

Table 2. Microprobe analyses and structural formulae for mordenite from the Prassa deposit, Kimolos.

	1 zone 5	2 zone 5	3 zone 5	4 zone 5
SiO_2	72.63	73.02	72.89	70.23
Al_2O_3	11.78	11.97	11.74	11.98
Fe_2O_3	n.d.	n.d.	n.d.	n.d.
MgO	n.d.	n.d.	n.d.	0.59
CaO	2.82	2.71	2.63	2.71
Na_2O	3.79	3.36	1.54	1.69
K_2O	n.d.	0.91	3.48	2.38
Total	91.02	91.97	92.28	89.58
Structural formulae based on 48 oxygens				
Structural cations				
Si	20.18	20.15	20.22	20
Al	3.86	3.89	3.84	4.02
Exchangeable cations				
Na	2.04	1.80	0.83	0.93
Ca	0.84	0.8	0.78	0.83
K	0	0.32	1.23	0.86
Mg	0	0	0	0.25
E (%)	3.68	4.64	5.94	1.73
Si/Al	5.23	5.18	5.27	4.98

E (%) = error value after Gottardi and Galli (1985). n.d. = not detected. See text for analytical details.

occasionally >50 (Figure 8). Three types of mordenite were recognized: (1) fibers (Figure 8a) <10 μm, which originate from an amorphous material, possibly an Al-Si gel; (2) well-formed, long fibers (arrow in Figure 8b), which often crystallize over the smectite substrate, and (3) fibers (Figure 8b) perpendicular to pore-spaces and cavities and linking the flanks of dissolved cavities. Finally, opal-CT occurs in the form of spherulitic crys-

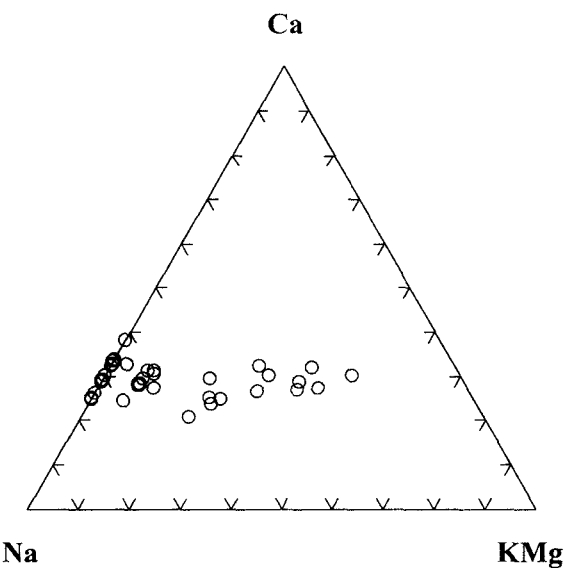

Figure 5. Compositional trends of mordenites with respect to the relative abundance of their exchangeable cations. The Mg content is low.

https://doi.org/10.1346/CCMN.2001.0490303 Published online by Cambridge University Press

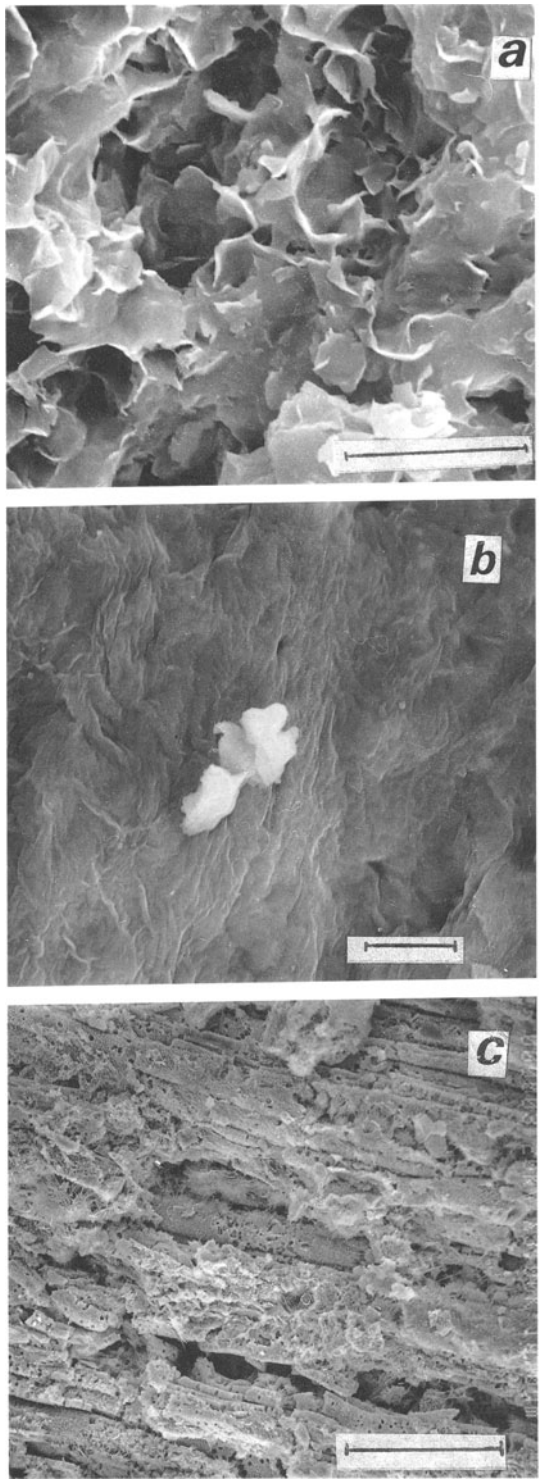

Figure 6. SEM images of smectite and mordenite from the Prassa deposit. (a) Smectite crystals with honeycomb texture. (b) Smectite flakes of a 'closed' texture which do not form the more 'open' honeycomb structures. The white phase in the center is a Si-Al-gel. (c) Pseudomorphic replacement of volcanic glass by smectite and mordenite (small fibrous crystals). The original texture has been preserved. Scale bars a = 6 μm, b = 10 μm, c = 150 μm.

tals, diagenetic by-products, formed by co-precipitation of silica during the formation of smectites. Axiolitic opal-CT, which is common in the bentonites from Milos, derived from acidic precursors (Christidis *et al.,* 1995), was not observed in this study.

Particle-size measurements

Length and width measurements of the smectite particles from the smectite- and the mordenite-bearing zone were plotted in histograms (Figure 9a, b). The size-distribution profiles are shifted towards greater length and width in the mordenite-bearing zone and the size-distribution profiles of samples SM277 and SM278 are comparable. The theoretical lognormal curves calculated from the particle-size distribution (PSD) data (Koch and Link, 1971) describe the size distribution profiles, because the χ^2 test indicates that the significance level of all distributions exceeds 20%. Therefore, all crystal-size distributions can be characterized as lognormal. The mean length and width of the smectite particles, along with the parameters α and β^2 (Eberl *et al.,* 1990), are listed in Table 3. Parameter α describes the mean of the natural logarithms of the observations (ω) and equals (Eberl *et al.,* 1990)

$$\alpha = \sum (\ln \omega) f(\omega) \quad (1)$$

and β^2 describes the variance of the natural logarithms of the observations and equals

$$\beta^2 = \sum [\ln(\omega) - \alpha]^2 f(\omega) \quad (2)$$

In equations (1) and (2), $f(\omega)$ is the frequency of the observation ω. The crystal-size distributions described by these parameters often have distinctive shapes, which can provide information about the crystal-growth history of various types of minerals (Baronnet, 1982; Eberl *et al.,* 1998).

The β^2 parameter of both length and width is nearly constant for all samples, whereas parameter α increases in the mordenite-bearing zone. This effect explains the lognormal steady-state shape profile observed when the PSDs were plotted in reduced coordinates (Figure 9c, d), because such PSD profiles are observed in crystal populations where β^2 remains constant with an increase in crystal size (parameter α). Lognormal profiles (Figure 10) with these characteristics may indicate crystal growth in supply-controlled open systems or supply-controlled random ripening in closed systems (Eberl *et al.,* 1998). Unlike Ostwald ripening (Baronnet, 1982), random ripening is not controlled by the surface area of the reactive particles but might be controlled by other factors such as strain or environmental heterogeneity (Eberl *et al.,* 1998). Note that bentonites form in open systems characterized by high water : rock ratios and remarkable microenvironmental heterogeneity (Christidis and Dunham, 1993; Christidis *et al.,* 1995). Analytical data throughout the alteration profile (Table 4) as well as from similar alter-

https://doi.org/10.1346/CCMN.2001.0490303 Published online by Cambridge University Press

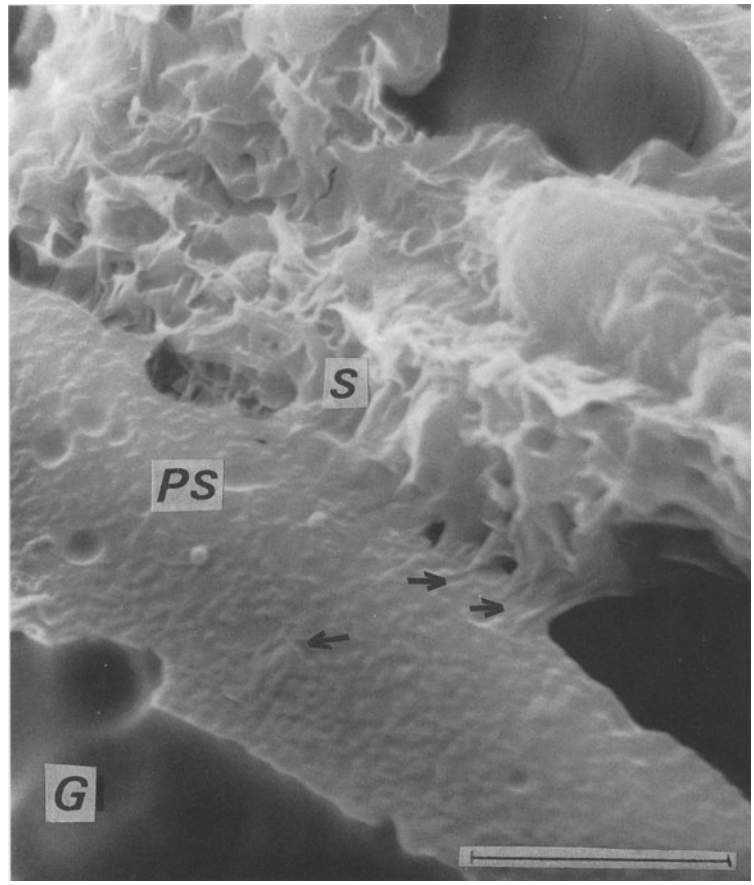

Figure 7. SEM image showing the progressive alteration of volcanic glass (G) to smectite (S) through an intermediate precursor phase (PS) of probable allophane composition (see text). The arrows indicate smectite flakes growing from the precursor. The small spherules present are opal-CT. Scale bar = 6 μm.

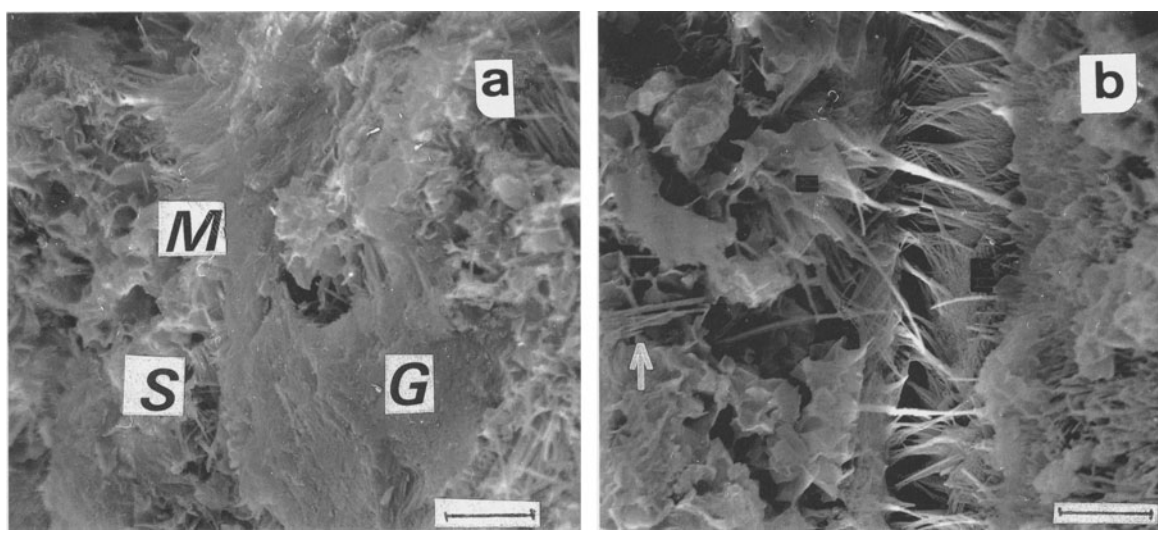

Figure 8. SEM images showing the different morphological types of mordenite: (a) mordenite fibers (M) forming from an amorphous, gel-like precursor (G), associated with smectite flakes (S). No direct association is observed between mordenite and smectite. (b) Well-developed mordenite fibers associated with smectite, joining cavity walls formed from the dissolution of the volcanic glass, and mordenite fibers (shown by white arrow) draped over smectite flakes. Scale bars = 10 μm.

https://doi.org/10.1346/CCMN.2001.0490303 Published online by Cambridge University Press

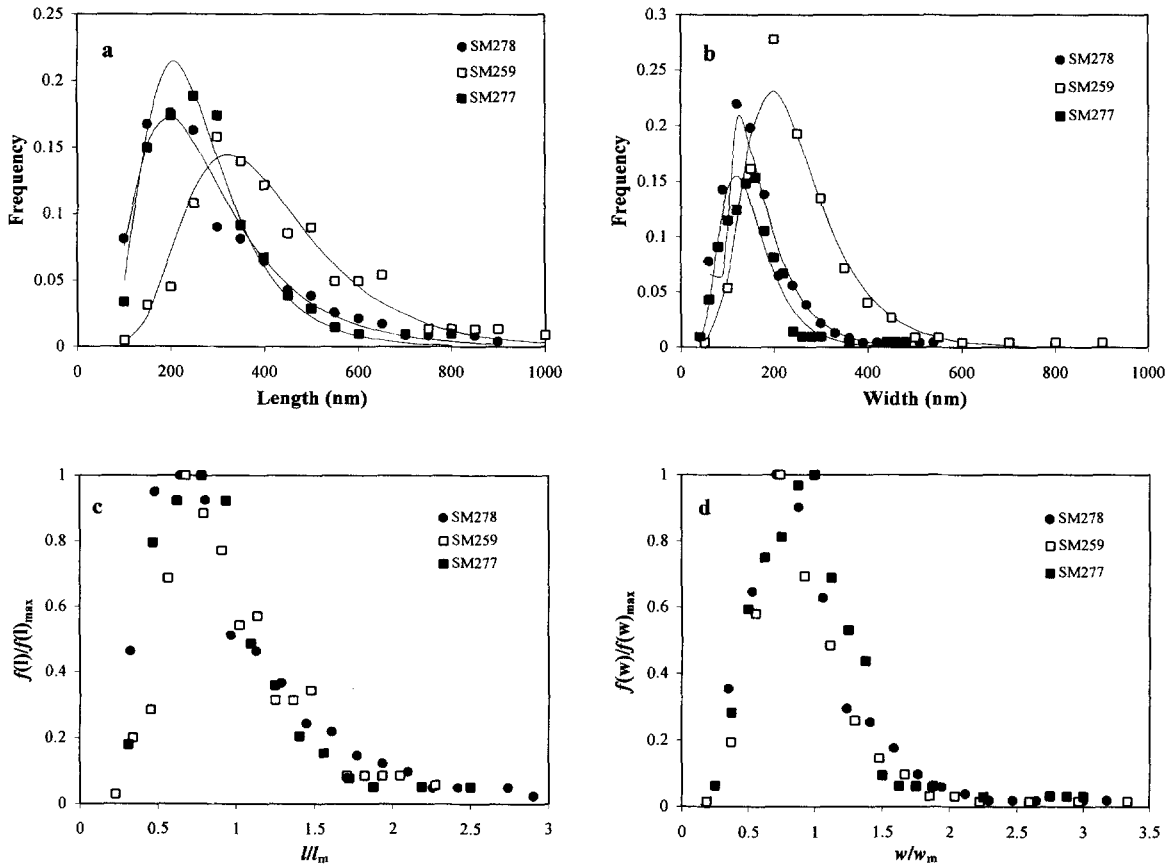

Figure 9. Particle-size distributions (PSDs) and corresponding reduced profiles for length (a and c) and width (b and d), of smectite particles from the smectite zone (SM278) and the mordenite-bearing zone (SM277 and SM259). The solid lines in (a) and (b) correspond to calculated lognormal distributions. $f(I)$ is the frequency of a given particle dimension, $f(I)_{max}$ is the maximum frequency encountered, l and l_m denote particle length and mean particle length, respectively and w and w_m denote particle width and mean particle width, respectively.

ation terrains suggest that this is also the case in this study (see below). Mass balance calculations for the smectite- and the mordenite-bearing zone indicated water:rock ratios of 13.3:1 and 5.5:1, respectively (Christidis, 1998a).

DISCUSSION

Formation and crystal growth of smectite

The coexistence of alteration zones with mordenite and smectite was used to examine the possible influence of zeolites on smectite growth. Smectite forms first during dissolution of the volcanic glass through nucleation and crystal growth, leading to pseudomorphic textures after volcanic glass (Figure 6c). The allophane-type precursor (Figure 7) either acts as a substrate or dissolves after reaction with the pore-fluid, so that smectite crystals nucleate rapidly under high local supersaturation conditions. Figures 9 and 10 suggest that smectite crystals continue to develop via supply-controlled growth in an open system or supply-controlled random ripening in a closed system. Lognormal size-distribution profiles are also exhibited by crystals

Table 3. Average values of length and width and α and β^2 parameters of the smectite particles from the smectite zone (SM278) and the mordenite-bearing zone (SM277 and SM259). α and β^2 are the mean and variance of the natural logarithms of the observations, respectively.

Sample	Smectite particle size		α		β^2	
	Length (μm)	Width (μm)	Length	Width	Length	Width
SM278	0.31 ± 0.16	0.17 ± 0.08	5.54	4.97	0.26	0.20
SM277	0.32 ± 0.13	0.16 ± 0.06	5.51	4.94	0.18	0.17
SM259	0.44 ± 0.17	0.27 ± 0.10	5.95	5.44	0.17	0.17

https://doi.org/10.1346/CCMN.2001.0490303 Published online by Cambridge University Press

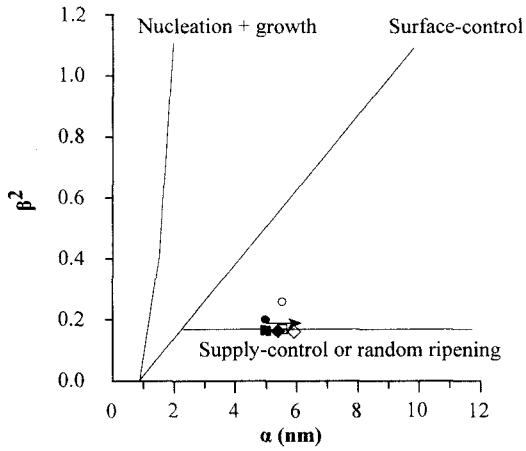

Figure 10. Variations in α and β^2 for PSDs of smectites from the smectite and the mordenite-bearing zone, plotted on Figure 12 of Eberl *et al.* (1998). The arrow indicates the direction of decrease of the water:rock ratio during alteration. Solid symbols denote length and open symbols denote width. Circles = SM278, squares = SM277, diamonds = SM259.

which grow via a surface-controlled growth mechanism (Eberl *et al.*, 1998). However, such systems yield PSDs with large variance (parameter β^2) at large mean crystal sizes (parameter α), because β^2 increases linearly with mean size (Figure 10). A surface-controlled growth mechanism might have been active at an early stage during which the lognormal profile was established, after which the crystals grew larger, preserving β^2. Such examples were presented by Eberl *et al.* (1998) for garnet and dolomite.

The PSD data in Figure 10 are supported strongly by geochemical evidence. In Table 3, X-ray fluorescence (XRF) analyses from Christidis (1998a) are given. The observed remarkable increase of the Mg and Fe content relative to the parent rock during alteration, particularly in the smectite zone, is not residual (Christidis, 1998a). Therefore the pore-fluids supplied significant amounts of Mg and Fe required for smectite formation, indicating a supply-sustained growth in an open system. This type of crystal growth is believed to predominate in smectites and bentonites. However, the existence of abundant mordenite indicates incomplete alkali leaching, suggesting that some domains of the rock behaved as essentially closed sub-systems, due to variations in permeability. In such micro-domains, random ripening of smectite might also have occurred. Thus, the growth of smectite crystals was affected by the microenvironmental conditions.

The smectite from the mordenite-bearing zone is larger than its counterparts from the smectite zone (Figure 9). However, the lower water:rock ratio calculated for this zone (Christidis, 1998a) suggests that smaller amounts of nutrients (Mg and Fe) were supplied by the fluid phase. Thus, the mordenite-bearing zone must be considered a separate system. The greater crystal size of smectite in this zone is attributed: (1) to the lower supersaturation with respect to smectite, due to limited Mg supply and leaching of alkalis (*i.e.* conditions which favor mordenite), in domains with limited fluid flow (essentially closed sub-systems); and/or (2) to random ripening, involving dissolution of initially-formed smectite crystals, during the formation and in the vicinity of mordenite-rich domains. Thus, the similar size of smectite particles in SM277, collected close to the boundary between zones 4 and 5 (Figure 1), and SM278, is attributed to the low mordenite content of SM277.

The smectites studied do not display significant compositional variation, suggesting that the sustained supply of Mg and Fe may have homogenized the pore-

Table 4. Chemical analyses of the rocks in the Prassa alteration profile and calculated water:rock (WR) ratios (after Christidis, 1998a).

	SM285	SM283	SM282	SM280	SM278	SM277	SM261
SiO_2	72.51	71.78	76.23	61.39	60.82	64.47	67.74
Al_2O_3	12.06	13.21	11.66	20.47	20.67	19.06	16.79
TiO_2	0.09	0.1	0.11	0.16	0.17	0.15	0.13
Fe_2O_3	0.56	0.72	1.17	1.91	2.18	1.63	1.19
MnO	0.01	0.02	0	0	0.01	0	0.02
MgO	0.27	1.33	2.79	5.09	5.28	3.41	1.99
CaO	0.51	0.61	0.7	1.1	1.06	1.08	1.14
Na_2O	3.51	3	0.39	0.75	0.88	1.17	1.94
K_2O	4.19	2.82	0.12	0.21	0.33	1.69	2.3
P_2O_5	0	0.02	0.02	0.02	0	0	0
LOI	5.84	5.86	6.1	7.85	6.91	7.43	7.29
SO_3	0	0	0.06	0.33	0.81	0	0
Total	99.55	99.47	99.35	99.28	99.12	100.09	100.53
WR ratio		4.5:1		13.3:1		5.5:1	

Sample SM285 corresponds to the fresh glass, SM283 to the glass + smectite zone, SM282 to the smectite + opal-CT zone, SM280 and SM278 to the smectite zone, and SM277 and SM261 to the smectite + mordenite zone. Characterization of the alteration zones is from Christidis and Scott (1997).

https://doi.org/10.1346/CCMN.2001.0490303 Published online by Cambridge University Press

fluid chemistry, forming smectite with increased Mg and Fe content compared with the parent rock. This explains the compositional characteristics observed in Figure 3. In contrast, the pore-fluid chemistry during the formation of the bentonites from Milos from similar parent rocks was significantly inhomogeneous, and its chemistry was dominated by small-scale uptake of Mg by the solid phase and by local migration of Mg, Fe and Si (Christidis and Dunham, 1997). Thus, unlike the bentonites from Milos, the chemistry of the protolith in the present study did not influence the crystal chemical characteristics of the neoformed smectites.

The use of length and width measuments of smectite particles instead of thickness measurements was not arbitrary. The thickness of a smectite layer is constant ("fundamental" particle size of 10 Å, Nadeau *et al.*, 1984) throughout the growth process, unlike interstratified illite-smectite, the particles of which become progressively thicker with illitization (Eberl *et al.*, 1990; Inoue and Kitagawa, 1994; Christidis, 1995). Smectite particles tend to form quasicrystals, the thickness of which depends on the type of the interlayer cation (Schramm and Kwak, 1982; Sposito, 1994). For Ca,Mg-rich smectites in this study, quasicrystals contain 3–7 layers (Schramm and Kwak, 1982; Sposito, 1994). Using Pt shadowing, Christidis (1995) found that the thickness of Ca,Mg-rich smectites from bentonites from Milos is 44 ± 11 Å. Therefore, unlike interstratified illite-smectite, the distribution of smectite particle thickness is not considered thermodynamically important and cannot provide a direct measure of the progress of smectite growth.

Influence of the smectite and mordenite on the pore-fluid chemistry

K-rich mordenite is an unusual mineral because the dominant exchangeable cations of this zeolite are Na and Ca (Gottardi and Galli, 1985). Clinoptilolite is favored over mordenite at low temperatures and high K:Na ratios in synthesis experiments (Hawkins, 1981). The exchangeable-cation chemistry of smectite is comparable with that of the coexisting K-rich mordenite (Figure 4). Smectite may have influenced the pore-fluid chemistry if the first particles to form contained interlayer K. If so, the $K^+/(Na^+ + Ca^{2+})$ activity ratio of the pore-fluid would have been relatively low, and the $(Na^+ + Ca^{2+})/H^+$ activity ratio high, favoring the formation of the Na,Ca-rich mordenite (common mordenite).

The formation of K-bearing phases was influenced by the pH of the fluid phase and/or the cooling history of the parent rock. Alteration in an open system, at neutral to slightly alkaline pH is expected to increase the Na^+/K^+ activity ratio in the pore-fluid relative to the parent rock, because Na is leached preferentially (White and Claasen, 1980) thereby raising the K^+/Na^+ ratio of the leached glass. Also, rapid cooling of the parent volcanic glass forms large interstices in the silicate network, thereby facilitating accommodation of K (Shiraki and Iijama, 1990). The K might participate in the formation of K-bearing smectite and subsequently K-bearing mordenite via dissolution of their poorly crystalline or amorphous precursors. At a later stage, reaction with the fluid phase, possibly modified seawater (Christidis, 1998a), led to replacement of K by Ca and Na, present in the fluid phase.

Alternatively, dissolution of K-bearing smectite crystals, and growth of Ca,Na-rich smectite via random ripening, in domains where the system was essentially closed, released K to the pore-fluid and removed Ca and Na from the pore-fluid, thereby raising the $K^+/(Na^+ + Ca^{2+})$ activity ratio. Thus, the microenvironment was favorable for the crystallization of K-rich mordenite. Note that Matsuda *et al.*, (1996) observed removal of interlayer K from smectite and concomitant formation of K-rich clinoptilolite with increasing depth, during diagenetic alteration of rhyolitic glass. These mechanisms do not require nucleation of smectite during zeolite formation, which would be unlikely due to the unfavorable pore-fluid chemistry. Moreover they do not require an external K influx for which there is no geological evidence.

Nevertheless, it is not clear why K-rich mordenite formed instead of clinoptilolite. Four possibilities are: (1) K-rich mordenite was favored by epitaxial growth over a Na- and Ca-rich precursor. Although such a 'zonal' relationship was not observed, it is not excluded because of restrictions of the microprobe analysis. (2) The temperature was suffiently high to favor the formation of mordenite over that of clinoptilolite. Mordenite, which may be a high-*T* analogue for clinoptilolite, is commonly found in high-*T* terrains, of either hydrothermal or geothermal origin (Boles, 1977). (3) The Al activity of the pore-solution was either high or low. At 25°C clinoptilolite has a maximum stability field at an intermediate Al activity, which decreases with either the increasing or decreasing activities of Al (Bowers and Burns, 1990). Indeed, the Si:Al ratio of mordenites is high (≤5.8:1) suggesting a small degree of Al activity. (4) The composition of the Si species in the pore-fluid may have favored the formation of mordenite. If the ratio of Si monomers [$Si(OH)_4$, $SiO(OH)^-$ or $SiO_2(OH)_2^{2-}$] to Si-tetramers [$Si_4O_8(OH)_4^{4-}$] increases, then Si pentamers (close to the five-membered ring structure of mordenite) might form (tetramer + monomer) (Hawkins, 1981). For pH <8.5, the alteration of rhyolitic glass yields predominantly $Si(OH)_4$ as a Si monomer, and a very high $Si(OH)_4$:$Al(OH)_4^-$ ratio (Mariner and Surdam, 1970). This suggests that the Al activity was low, *i.e.* not suitable for the formation of clinoptilolite.

SUMMARY AND CONCLUSIONS

The progressive alteration of a rhyolite glass to a typical bentonite and a mordenite-bearing bentonite in

https://doi.org/10.1346/CCMN.2001.0490303 Published online by Cambridge University Press

Kimolos Island, Greece, provided valuable information about the mechanism of formation and growth of smectite. The smectites formed are Chambers- and Tatatilla-type montmorillonites, they display rather insignificant compositional variation and seem to have nucleated from a poorly crystalline precursor, which had an allophane-type composition. Mordenite has also formed at the expense of an Al-Si rich amorphous material.

Length and width measurement of smectites yielded lognormal profiles, which suggest supply-controlled crystal growth in open system or random ripening in closed system. Supply-controlled crystal growth in an open system is supported by mass balance calculations in previous studies, which show that large amounts of Mg and Fe have been transported by the fluid phase (Christidis, 1998a). Both smectite and mordenite can affect pore-fluid chemistry by ion exchange reactions. Moreover, random ripening of unstable montmorillonite crystals in semi-closed domains of the system is expected to release K, favoring the formation of K-mordenite. Exchange of K between smectite and zeolites, often present in bentonites, may be an important factor for retaining K in the system, which in turn can facilitate illitization, during subsequent diagenesis. Such a mechanism might provide a plausible explanation for K availability, which affects the smectite-to-illite reaction, in terrains where evidence for a source of K is lacking and zeolites are present.

ACKNOWLEDGMENTS

The constructive comments and suggestions of J. Środoń, J. Boles, W.C. Elliott and S. Guggenheim improved the text. I am indebted to A. Low and E. Roberts of the Biology Department, University of Leicester, for their help with the TEM.

REFERENCES

Altaner, S.P. and Grim, R.E (1990) Mineralogy, chemistry and diagenesis of tuffs in the Sucker Creek Formation (Miocene), Eastern Oregon. *Clays and Clay Minerals,* **38,** 561–572.

Banfield, J.F. and Eggleton, R.A. (1990) Analytical Transmission Electron Microscope studies of plagioclase, muscovite, and K-feldspar weathering. *Clays and Clay Minerals,* **38,** 77–89.

Banfield, J.F., Jones, B.R. and Veblen, D.R. (1991) An AEM-TEM study of weathering and diagenesis, Albert Lake, Oregon: I. Weathering reactions in the volcanics. *Geochimica et Cosmochimica Acta,* **55,** 2781–2793.

Baronnet, A. (1982). Ostwald ripening: The case of calcite and mica. *Estudios Geologicos,* **38,** 185–198.

Boles, J.R. (1977) Zeolites in low-grade metamorphic rocks. Pp. 103–135 in: *Mineralogy and Geology of Natural Zeolites* (F.A. Mumpton, editor). Reviews in Mineralogy, **4.** Mineralogical Society of America, Washington, D.C.

Bowers, T.S. and Burns, R.G. (1990) Activity diagrams for clinoptilolite: Susceptibility of this zeolite to further diagenetic reactions. *American Mineralogist,* **75,** 601–619.

Cas, R.A.F. and Wright, J.V. (1988) *Volcanic Successions. Modern and Ancient.* Unwin Hyman, London, 528 pp.

Christidis, G. (1995) Mechanism of illitization of bentonites in the geothermal field of Milos Island, Greece. Evidence based on mineralogy, chemistry, particle thickness and morphology. *Clays and Clay Minerals,* **43,** 567–594.

Christidis, G. (1998a) Comparative study of the mobility of major and trace elements during alteration of an andesitic and a rhyolitic rock to bentonite in the islands of Milos and Kimolos, Aegean, Greece. *Clays and Clay Minerals,* **46,** 379–399.

Christidis, G. (1998b) Physical and chemical properties of some bentonite deposits of Kimolos Island, Greece. *Applied Clay Science,* **13,** 79–98.

Christidis, G. and Dunham, A.C. (1993) Compositional variations in smectites: Part I. Alteration of intermediate volcanic rocks. A case study from Milos Island, Greece. *Clay Minerals,* **28,** 255–273.

Christidis, G. and Dunham, A.C. (1997) Compositional variations in smectites: Part II. Alteration of acidic precursors. A case study from Milos Island, Greece. *Clay Minerals,* **32,** 253–270.

Christidis, G. and Scott, P.W. (1997) Origin and colour properties of the white bentonites. A case study from the Aegean Islands of Milos and Kimolos, Greece. *Mineralium Deposita,* **32,** 271–279.

Christidis, G., Scott, P.W. and Marcopoulos, T. (1995) Origin of the bentonite deposits of Eastern Milos, Aegean, Greece. Geological, mineralogical and geochemical evidence. *Clays and Clay Minerals,* **43,** 63–77.

Eberl, D.D., Środoń, J., Kralik, M., Taylor, B.E. and Peterman, Z.E. (1990) Ostwald ripening of clays and metamorphic minerals. *Science,* **248,** 474–477.

Eberl, D.D., Drits, V.A. and Środoń, J. (1998) Deducing growth mechanisms for minerals from the shapes of crystal size distrubutions. *American Journal of Science,* **298,** 499–533.

Fyticas, M. and Vougioukalakis, G. (1993) Volcanic structure and evolution of Kimolos and Polyegos (Milos Island group). *Bulletin of the Geolological Society of Greece,* **28,** 221–237.

Fyticas, M., Innocenti, F., Kolios, N., Manetti, P., Mazzuoli, R., Poli, G., Rita, F. and Villari, L. (1986) Volcanology and petrology of volcanic products from the island of Milos and neighbouring islets. *Journal of Volcanology and Geothermal Research,* **28,** 297–317.

Gottardi, G. and Galli, E. (1985) *Natural Zeolites.* Springer-Verlag, Berlin, 409 pp.

Grim, R.E. and Güven, N. (1978) *Bentonites.* Elsevier, New York, 256 pp.

Güven, N. (1988) Smectite. Pp. 497–559 in: *Hydrous Phyllosilicates* (S.W. Bailey, editor). *Reviews in Mineralogy,* **19.** Mineralogical Society of America, Washington, D.C.

Güven, N. and Pease, R.W. (1975) Electron optical investigations on montmorillonites—II: Morphological variations in the intermediate members of the montmorillonite-beidellite series. *Clays and Clay Minerals,* **23,** 187–191.

Hawkins, D.B. (1981) Kinetics of glass dissolution and zeolite formation under hydrothermal conditions. *Clays and Clay Minerals,* **29,** 331–340.

Hay, R.L. (1977) Geology of zeolites in sedimentary rocks. Pp. 53–64 in: *Mineralogy and Geology of Natural Zeolites* (F.A. Mumpton, editor). *Reviews in Mineralogy,* **4.** Mineralogical Society of America, Washington, D.C.

Hay, R.L. and Guldman, S.G. (1987) Diagenetic alteration of silicic ash in Searles lake, California. *Clays and Clay Minerals,* **35,** 449–457.

Hess, P.C. (1966) Phase equilibria of some minerals in the K_2O-Na_2O-Al_2O_3-SiO_2-H_2O system at 25°C and 1 atmosphere. *American Journal of Science,* **264,** 289–309.

https://doi.org/10.1346/CCMN.2001.0490303 Published online by Cambridge University Press

Iijima, A. (1980) Geology of natural zeolites and zeolitic rocks. *Proceedings of the 5th International Conference on Zeolites,* pp. 103–118.

Inoue, A. and Kitagawa, R. (1994) Morphological characteristics of illitic clay minerals from a hydrothermal system. *American Mineralogist,* **79,** 700–711.

Kawano, M. and Tomita, M. (1992) Formation of allophane and beidellite during hydrothermal alteration of volcanic glass below 200°C. *Clays and Clay Minerals,* **40,** 666–674.

Koch, G.S. Jr. and Link, R.F. (1971) *Statistical Analysis of Geological Data.* Dover, New York, 335 pp.

Mariner, R.H and Surdam, R.A. (1970) Alkalinity and formation of zeolites in saline alkaline lakes. *Science,* **170,** 977–980.

Matsuda H., O'Neil, J.R., Jiang, W.T. and Peacor, D.R. (1996) Relation between interlayer composition of authigenic smectite, mineral assemblages, I/S reaction rate and fluid composition of silicic ash of the Nankai Trough. *Clays and Clay Minerals,* **44,** 443–459.

Nadeau, P.H., Tait, J.M., McHardy, W.J. and Wilson, M.J. (1984) Interstratified XRD characteristics of physical mixtures of elementary clay particles. *Clay Minerals,* **19,** 67–76.

Schramm, L.L. and Kwak, J.C.T. (1982) Influence of exchangeable cation composition on the size and shape of montmorillonite particles in dilute suspensions. *Clays and Clay Minerals,* **30,** 40–48.

Senkayi, A.L., Dixon, J.B., Hossner, L.R., Abder-Ruhman, M. and Fanning, D.S. (1984) Mineralogy and genetic relationships of tonstein, bentonite and lignitic strata in the Eocene Yegna Formation of East-Central Texas. *Clays and Clay Minerals,* **32,** 259–271.

Sheppard, R.A. and Gude, A.J. 3rd (1973) Zeolites and associated authigenic silicate minerals in tuffaceous rocks of the Big Sandy Formation, Mohave County, Arizona. *U.S. Geological Survey Professional Paper* **830,** 36 pp.

Shiraki, R. and Iiyama, T. (1990) Na-K ion exchange reaction between rhyolitic glass and (Na,K)Cl aqueous solution under hydrothermal conditions. *Geochimica et Cosmochimica Acta,* **54,** 2923–2931.

Sposito, G. (1994) The diffuse-ion swarm near smectite particles suspended in 1:1 electrolyte solutions: Modified Gouy-Chapman theory and quasicrystal formation. Pp. 128–155 in: *Clay-Water Interface and its Rheological Implications* (N. Güven and R. Pollastro, editors). Workshop Lectures, Vol. **4.** The Clay Minerals Society, Boulder, Colorado.

Steefel, C.I. and van Cappellen, P. (1990) A new kinetic approach to modeling water-rock interaction: The role of nucleation, precursors and Ostwald ripening. *Geochimica et Cosmochimica Acta,* **54,** 2657–2677.

Warren, E.A. and Ransom, B. (1992) The influence of analytical error upon the interpretation of chemical variations in clay minerals. *Clay Minerals,* **27,** 193–209.

White, A.F. and Claasen, H.C. (1980) Kinetic model for the short-term dissolution of a rhyolitic glass. *Chemical Geology,* **28,** 91–109.

Zhou, Z. and Fyfe, W.S. (1989) Palagonization of basaltic glass of DSPD Site 335, Leg 37: Textures, chemical composition and mechanism of formation. *American Mineralogist,* **74,** 1045–1053.

E-mail of corresponding author: christid@mred.tuc.gr

(Received 31 January 2000; revised 17 November 2000; Ms. 424; A.E. W. Crawford Elliott)

https://doi.org/10.1346/CCMN.2001.0490303 Published online by Cambridge University Press